Hindawi
International Journal of Antennas and Propagation
Volume 2023, Article ID 2543923, 12 pages
https://doi.org/10.1155/2023/2543923

Research Article

Design of Metamaterial Antenna Based on the Mathematical Formulation of Patch Antenna for Wireless Application

S. Prasad Jones Christydass,[1] **S. Suresh Kumar**,[1] **V. S. Nishok**,[1] **R. Saravanakumar**,[2] **S. Devakirubakaran**,[3] **J. Deepa**,[4] **and K. Sangeetha**[5]

[1]*Department of Electronics and Communication Engineering, QIS College of Engineering and Technology, Vegamukkapalem, Andhra Pradesh, India*
[2]*Department of Wireless Communication, Institute of ECE, Saveetha School of Engineering, Chennai, Tamilnadu, India*
[3]*Department of Electrical and Electronics Engineering, QIS College of Engineering and Technology, Vegamukkapalem, Andhra Pradesh, India*
[4]*Department of Electronics and Communication Engineering, K. Ramakrishnan College of Technology, Tiruchirappalli, Tamilnadu, India*
[5]*Department of Computer Science and Engineering, Kebri Dehar University, Kebri Dehar, Ethiopia*

Correspondence should be addressed to K. Sangeetha; sangeethak@kdu.edu.et

Received 31 October 2022; Revised 25 December 2022; Accepted 22 March 2023; Published 27 April 2023

Academic Editor: Paras Chawla

Copyright © 2023 S. Prasad Jones Christydass et al. This is an open access article distributed under the Creative Commons Attribution License, which permits unrestricted use, distribution, and reproduction in any medium, provided the original work is properly cited.

For WLAN/WIMAX applications, a brand-new tree-shaped metamaterial-loaded microstrip antenna is suggested. The reduced ground plane size and 4.4 dielectric constant (r) and 0.02 loss tangent (δ) dielectric are used to manufacture the $15 \times 16 \times 1.6\,mm^3$ microstrip antenna. Two X-shaped slots are added to achieve the characteristics needed for WIMAX applications at 5.5 GHz. Additionally, a split-ring resonator is added to the structure to increase its bandwidth. It runs for WLAN applications with a center frequency of 5.8 GHz. The proposed structure's measured impedance bandwidth is 45.39% with SRR and 53.48% without SRR, respectively. The proposed antenna is capable of satisfying the major requirements of modern wireless devices such as multiband operation, compact size, large bandwidth, and planar structure. The best outcomes are attained with the aid of parametric analysis of feed width, ground height, and slot width. All electromagnetic simulations were performed using CST Studio software. The measured results and the simulation agree. The waveguide extraction approach is used to demonstrate the SRR's permeability property. The suggested antenna had adequate impedance matching, was small, and had a wide bandwidth.

1. Introduction

Modern wireless communication systems like Bluetooth, WIFI, WLAN, WiMAX, etc. are integrated into small, portable communication devices nowadays, and the design of a downsized antenna with enough bandwidth capacity is the actual problem [1, 2]. The monopole antenna is the best option in these situations since it may provide a small size at a cheap cost and is easily etched on a single FR4 substrate. The literature has a number of designs aimed towards wireless applications. Our goal is to create an antenna with enough bandwidth for WLAN/WIMAX applications. The introduction of the ground strip and slit [3], the use of the meta surface as superstrate [4], bioelectric loading [5], the metamaterial [6], the use of the ZOR as a parasitic element [7, 8], the CPs impedance tuner [9], and the LC fractal resonator [10, 11], among other techniques, are all reported in the literature as ways to increase bandwidth. The above conventional method is capable of achieving good bandwidth, but each has its own demerits. Adding of slits and slots change the frequency response and creates an unstable radiation pattern; additional structures such as superstrate and parasitic patches lead to an increase in size, whereas fractal structure leads to fabrications difficulties.

Negative permittivity and permeability are qualities that are not commonly seen in natural materials and are instead obtained from their structure as opposed to their components. A metamaterial is an electromagnetic structure of that type. The remarkable electromagnetic characteristics of metamaterials are positively influencing the propagation direction of electromagnetic waves. The design of antenna [12, 13], filters [14–16], communication equipment [15, 16], and couplers [16] may all be done using metamaterials. The metamaterials are artificial electromagnetic structures with Pg/4 unit cells that behave like physical materials and have well-defined sequential properties [17]. Researchers are very interested in using metamaterials to improve antenna performance because of their distinctive electromagnetic activity. Some types of metamaterials include the split ring resonator (SRR) [18], omega-shaped [19], and complementary split ring resonator (CSRR) [20–23]. These materials are used to reduce size, improve bandwidth, and match impedance well. Since the SRR has a lower wavelength than its size due to its quasi-static resonant nature, it may be utilized to create tiny antennas.

In recent decades, wireless communication has grown tremendously due to the developments in technology. This attracts people to switch to smart electronic devices for basic needs like mobile phones, smart watches, fitness bands, security systems, and so on. Also, wireless communication played a vital role in military and satellite applications. These developments use strong wireless signals which suppress the weaker signals and also create noise, ineffective transmissions, and signal distortions. It should be guaranteed in the design of the antenna to work efficiently under any kind of transmission. This increases the performance of wireless devices in terms of efficiency, reliability, and flexibility. The use of more smart devices leads to the requirement for antennas that can be used for a wide range of applications. Hence, a wideband antenna with good impedance matching is the major requirement of all modern wireless devices. For achieving wide bandwidth, the techniques discussed above are widely utilized, but it leads to various pullbacks such as increased design complexity, distorted radiation pattern, and lower gain. This requirement leads to the requirement for an antenna that has wide bandwidth, radiates evenly, and has a reasonable gain. So we designed the antenna with the help of a metamaterial structure that can satisfy the major requirement of the modern wireless device. The objective of this proposed work is to develop an antenna for the WLAN/WIMAX applications with increased efficiency under the limiting factors discussed above.

For WLAN/WIMAX applications, a tree-shaped monopole microstrip antenna is suggested. A decreased ground plane aids in obtaining a good impedance match. The suggested structure's bandwidth was increased by adding the SRR to the substrate's bottom extremity. The proposed antenna's resonant properties are altered with the addition of the SRR. The study is done on SRR's negative permeability feature. To get the desired outcome, a parametric study of the feed width, slot width, and ground height is conducted.

The structure of the paper is as follows: Section 1 describes the step-by-step procedures of the metamaterial antenna with the enriched bandwidth. Section 2 describes the step-by-step simulation with the required mathematical expressions and derivative parts of the effective permeability, refractive index, and permittivity of the metamaterial structure. It also describes the fabrication procedure of the proposed antenna and the supporting data. Section 3 describes the parametric study of the proposed antenna and the corresponding comparison results. Section 4 describes the extraction of the permeability property of SRR and Section 5 discusses the results obtained from the proposed antenna. Also, a comparison of results between the proposed antenna and the existing advanced antennas were presented. In Section 6, the paper has concluded the research work based on the effectiveness and advantages of the proposed antenna.

2. Mathematical Design Methodology and Simulation

The radiating element with SRR at the bottom of the substrate is supplied by a 50-ohm microstrip line. Based on research and a review of the literature, we propose a low-profile, multipurpose, small-sized, low-frequency band with and without a metamaterial antenna. The radiating patch, antenna substrate, and ground plane are the three layers of the antennas, and their design is carried out at a millimeter (mm) scale. The initial design equations for the embedded metamaterial and slots in the ground are as follows:

$$M_W \approx M_L \approx \frac{L_S}{5.25} \approx \frac{W_S}{4},$$
$$S_W \approx \frac{L_g}{3} \approx \frac{W_g}{10.67} \approx \frac{S_W}{1.33}, \tag{1}$$

where S_H is the length of the slot and S_W is the width of the slot in the ground plane, and M_W and M_L are the length and breadth of the metamaterial unit cell in the patch. The mathematical calculations used to begin the design of the proposed antenna may be obtained from basic theoretical equations as follows. The value for the dielectric constant can be expressed as the following equation:

$$\varepsilon_{re} \approx \frac{\varepsilon_r + 1}{2} \approx \frac{\varepsilon_r - 1}{2}\left(1 + \frac{12h}{w}\right)^{-0.5}. \tag{2}$$

Due to the electric field acts on the antenna, the dimensions will be changed which can be said as fringing length, ΔL and this can be expressed as in the following equation:

$$\Delta L \approx 0.412\left\{\frac{(\varepsilon_{re} + 0.30)\,((w/h) + 0.26)}{(\varepsilon_{re} - 0.258)\,((w/h) + 0.80)}\right\}h. \tag{3}$$

The fundamental frequency of the antenna with respect to the dielectric field and the fringing length can be written as the following equation:

$$f_1 \approx \frac{c}{2(L + \Delta L)\sqrt{\varepsilon_{re}}}, \tag{4}$$

where "w" denotes the width of the antenna element and "h" denotes the height of the substrate material, and "ϵr" denotes the dielectric constant of the FR4 substrate, which is 4.40. The antenna element's size and shape are determined by the following expressions:

$$L \approx \frac{\lambda_0}{2\sqrt{\varepsilon_r}} - 2\Delta L \approx \frac{c_0}{2f_0\sqrt{\varepsilon_r}} - 2\Delta L,$$
$$W \approx \frac{\lambda_0}{2}\sqrt{\frac{\varepsilon_r + 1}{2}} \approx \frac{c_0}{2f_0}\sqrt{\frac{\varepsilon_r + 1}{2}}. \quad (5)$$

Based on these parameters, the dimensions, like length and width, fundamental frequency, permeability, permittivity, and other constrains were calculated for the design of the proposed method. Figure 1 shows the top and bottom views of the suggested antenna. All three antennas' designs are depicted in Figure 2, and their parameter dimensions are reported in Table 1. Figure 3 depicts the constructed antenna's snap.

The proposed antenna dimensions are given in Table 1. The top view and the bottom view of the proposed antenna are shown in Figure 1. The dimension of the proposed antenna is nearly 16 mm × 15 mm. The size of the proposed antenna is captured by an Indian one-rupee coin where the antenna size is smaller than this coin. The proposed antenna has a tree-shaped structure; initially, a circular patch is designed, and later it is converted into a tree-shaped antenna. The tree-shaped antenna is designed by merging the ½ and ¾ th of the actual initial size of the circular patch. The discontinuities at the edges lead to a change in current direction which in turn leads to a good impedance band width match without increasing the size. The proposed antenna's overall size remained the same, yet its bandwidth significantly improved due to enhancements made to its structure. The major significant impact of the structure's improvement in bandwidth without the increase in overall footprint of the proposed antenna. The antenna geometry is designed with computer assistance in the initial stage. The mask is made from a negative print of this geometry on translucent sheet. Using acetone, a double-sided copper-clad substrate FR4 with the proposed dimensions was completely cleaned. The etched pattern is disrupted by dust or other contaminants on the copper-clad surface, changing the resonance frequency. The second process involves laminating a negative photoresist layer to the dry and clean copper-clad substrate. The photoresist laminated copper-clad substrate is securely adhered to the negative mask that was created in the first phase. UV light is shone upon the copper-clad substrate that has been mask and photoresist-laminated. The third step is to develop the copper-clad substrate with a UV-exposed photoresist laminate. Unexposed photoresist is light blue and disintegrates in the developer solution, but photoresist that has been exposed to UV radiation hardens and becomes a dark blue colour. As a developer, sodium carbonate is employed. Finally, a solution of ferric chloride (FeCl3) is used to chemically etch the produced copper-clad substrate. Except for below the firm photoresist, the copper components disintegrate in FeCl3. To get rid of any remaining etchant, the etched substrate is washed under running water and dried. Use of sodium hydroxide is used to remove the hardened photoresist. The effective microstrip antenna has been fabricated, and the performance of this antenna has been analyzed in various aspects and its corresponding results were presented and discussed as follows.

Antenna A is a tree-shaped antenna; Antenna B is a tree-shaped antenna with an X slot; and Antenna C is a tree-shaped antenna with an X slot and an SRR. Broadband from 5 GHz to 11 GHz is produced by Antenna A, with a maximum return loss of −35 dB. To achieve effective impedance matching, antenna A incorporates a smaller ground plane. The radiating element of antenna B has two X-shaped slots that it uses to produce 5.5 GHz resonance. Its operational frequency range is 4.507 GHz to 7.0126 GHz, with a maximum s11 of −29.651 dB and a 45.39% bandwidth of percentage impedance. To create antenna C, an SRR is inserted into the substrate bottom at the top right corner. Antenna C has a wider bandwidth and a 5.8 GHz resonating frequency. Antenna C's impedance bandwidth as a percentage is 53.48%. While antenna C may be used for WLAN applications, antenna B, which has two X-shaped slots, can be utilized for WIMAX applications.

It is crucial to pick the best-driven solution, the right feeding mechanism, a fine-mesh structure, and the required electromagnetic boundary conditions in order to provide a converged solution for the specified design. The predicted successes in terms of return loss, gain, S-parameter, and radiation patterns of the metamaterial embedded antenna have been examined and numerically improved. To estimate the effective permittivity (εr), permeability (μr), and refractive index (nr) for the suggested metamaterial structure integrated into the antenna structure, reflection (S11) and transmission (S21) coefficients are obtained.

Figure 4 shows the simulated s11 vs. frequency result. Antenna B has a band resonating at 5.5 GHz with an impedance bandwidth of 2.5089 GHz, which suggests that antenna A has a noticeably large bandwidth from 5 GHz to 11 GHz. Additionally, C now has a wider bandwidth with a central frequency of 5.8 GHz thanks to the SRR antenna. Due to the shift in current flow direction along the SRR, the resonance frequency is increased once the SRR is introduced at a higher frequency.

Antenna C's surface current distribution is seen in Figure 5. The current is concentrated near the SRR at 5.8 GHz. The surface current displayed in Figure 5 clearly shows that the current is maximum concentrated in the split ring resonator which is printed in the back of the ground. The SRR is induced by the field produced by the patch, and the presence of SRR alters the current direction which is responsible for the 5.8 GHz.

Table 2 compares the proposed antenna's performance to that of an existing antenna from the literature. Table 2 indicates that the suggested antenna has a compact size, and this work also analyses the metamaterial characteristic. Also, the properties and performance of the proposed antenna have been analyzed and compared with some of the advanced antennas discussed in the literature [24, 25] in terms

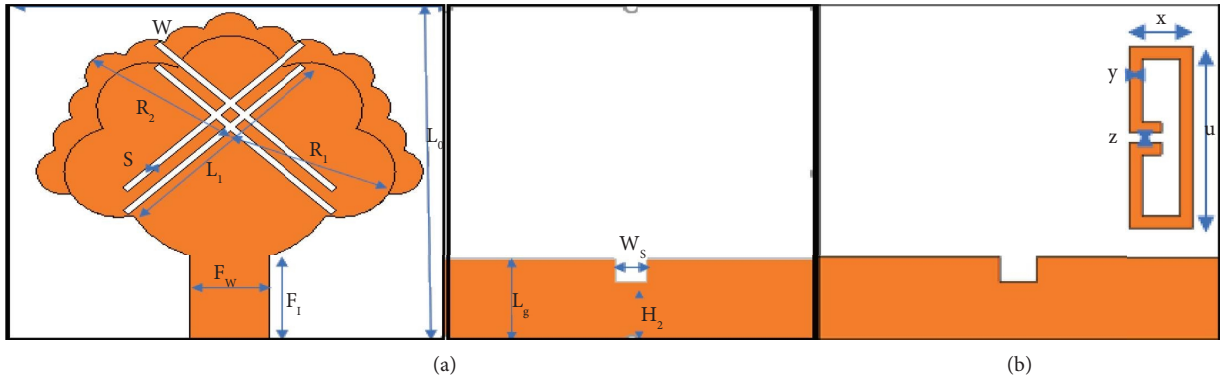

Figure 1: (a) Antenna B-front and back view. (b) Antenna C back view.

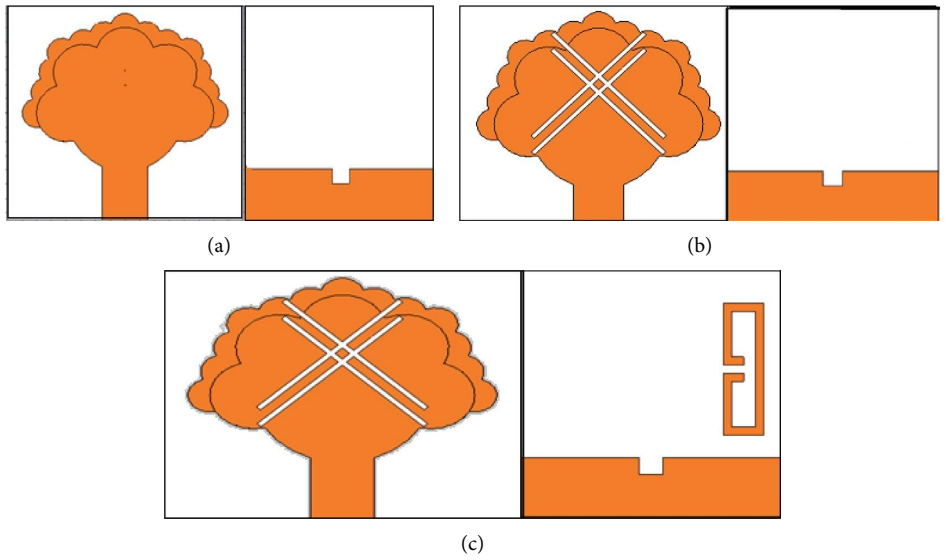

Figure 2: Evolution stage geometry. (a) Antenna A. (b) Antenna B. (c) Antenna C.

Table 1: Dimension of antenna C.

Parameters	Size (mm)
W	16
L	15
L_1	1.61
F_1	6.5
F_W	2.9
S	0.25
L_g	3.6
R_1	6
R_2	7
H_2	2.6
H	1.6
T	0.035
W_s	0.725
u	8
x	2
$y = z$	0.5

of no of elements used for the construction, dimension, frequency range, bandwidth, and method used for the construction. The antenna proposed in [24] has the least bandwidth among the other antennas taken for the comparison. The dimensions of this antenna are 26 mm × 23.6 mm. It is a kind of microstrip antenna, but its metamaterial property has not been verified in any kind of analysis. In [25, 26], a MIMO antenna is proposed for dual-band antenna with wide bandwidth which covers all the wireless application; in [27], fractal geometry is presented to have a bandwidth of 550 MHz; in [28], a taperer patch with truncated ground is proposed to have a wide bandwidth from 3.11 to 7.3 GHz; and in [29],a dipole is presented which operates at single band from 5.7 to 5.9 GHz. In [30], the multidesign antenna is capable of resonating at three different bands. The antenna consists of three different shapes, which in turn operate at three different frequencies. In [31], a rectangular resonator is presented for RFID application, but its operating frequency has a very narrow bandwidth. An inset-fed antenna for wireless applications is presented in [32] with a complex design and operating in a narrow band. In [33], a flexible dual narrow band antenna is presented for wireless application. The proposed antenna B and the proposed antenna C have the same dimensions of

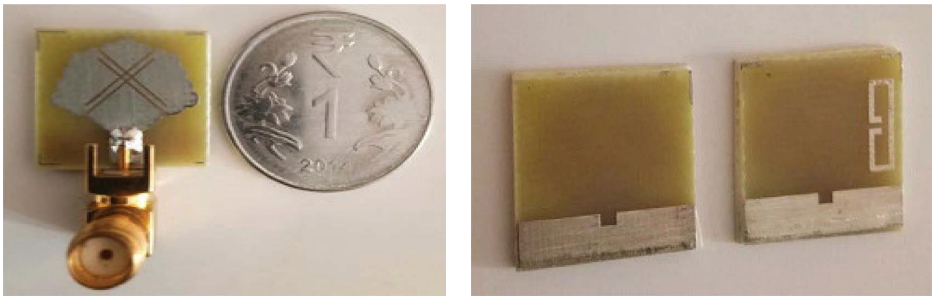

(a) (b)

Figure 3: Proposed antenna. (a) Antenna with SMA connector. (b) Back view of antenna B and C.

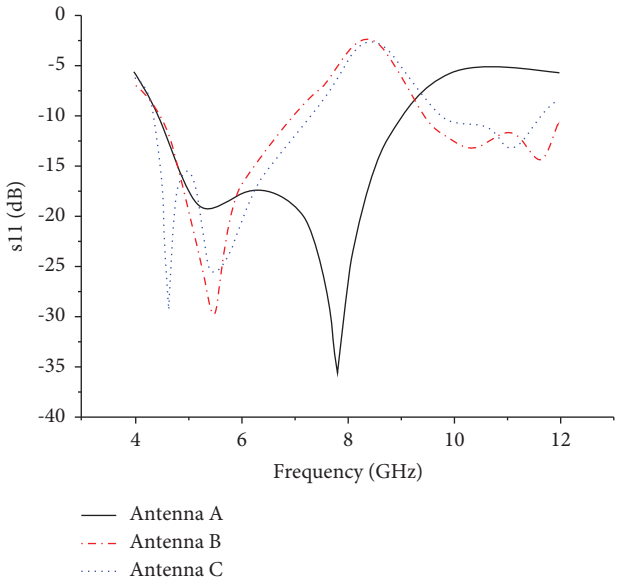

Figure 4: Return loss comparison plot.

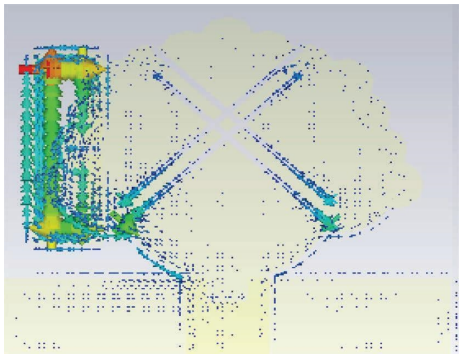

Figure 5: 5.8 GHz @ proposed antenna surface current.

16 mm × 15 mm. The bandwidth of antenna C is 0.5 MHz greater than that of the type B antenna. Also, antenna C has an upper frequency of 4.4238 GHz and a lower frequency of 7.3451 GHz, whereas antenna B has an upper frequency of 4.4712 GHz and a lower frequency of 7.0126 GHz.

In contrast to the antennas presented in the comparison, the suggested antenna's metamaterial property has been confirmed by the appropriate study. This guarantees that the suggested antenna will be dependable and best appropriate for real-time applications. The proposed antenna is capable of having a large bandwidth which is a major requirement of the wireless application. With large bandwidth, the data rate requirements of the wireless application are easily satisfied. The applications which are severed by this proposed antenna are WIFI, WLAN, and WiMAX.

3. Proposed Antenna Parametric Analysis

The antenna C parametric research aids in determining the ideal value. The ground's feed width (Fw), slot width (Ws), and ground height (Lg) are the subjects of the investigation. The bandwidth comparison between the various types of antennas and the proposed method is shown in Figure 6.

Figure 7 shows the variation in feed width (Fw) from 2.8 mm to 3 mm in increments of 0.1 mm. The optimal value of Fw is determined to be 2.9 because it ensures adequate impedance matching throughout the full working range while increasing the bandwidth.

The research also uses the width of the ground slot to determine the best value for it by adjusting its value from 0.715 mm to 0.735 mm in stages of 0.01 mm. The suggested antenna displays a satisfactory return loss characteristic, as shown in Figure 8 when the slot width Ws is increased and the ideal value of 0.725 mm is chosen.

The ground height is adjusted from 3.4 to 3.8 mm in increments of 0.2 mm; the ground height of 3.6 mm is selected because it has a decent return loss plot, good impedance, and a respectable bandwidth improvement, as can be seen in Figure 9.

4. Waveguide Extraction Method

According to Pendry, a split-ring resonator is a well-known mu negative material. Due to the SRR's capacitive behaviour at low frequencies, the applied and induced magnetic fields will be in phase. SRR can have a permeability value greater than 1, and as a result, it mimics the magnetic dipole. Figure 10 shows the waveguide setup for the extraction permeability property. Figure 11 displays the magnitude and

Table 2: Proposed antenna vs. existing antenna (in literature).

Ref Nos.	No. of elements	Upper frequency (GHz)	Lower frequency (GHz)	Bandwidth (MHz)	Dimension (mm^2)	Method used	Metamaterial property verified
[24]	2	5.75	5.84	90	26×23.6	MIMO	Not verified
[25]	2	5.7	36.1	400	126×70	MIMO	Not verified
[26]	2	5.75	5.85	100	36×30	MIMO	Not verified
[27]	1	5.3	5.85	550	59×90	Fractal	Not verified
[28]	1	3.11	7.3	4190	25×28.5	Tranucated ground + tapared patch	Not verified
[29]	1	5.7	5.9	200	15×70	Dipole	Not verified
[30]	1	2.3	2.5	200	30×30	Capacitive loaded line resonator	Not verified
Proposed antenna B	1	4.47	7.012	2541	16×15	X-shaped slot	Verified
Proposed antenna C	1	4.42	7.345	2921	16×15	X-shaped slot + SRR	Verified

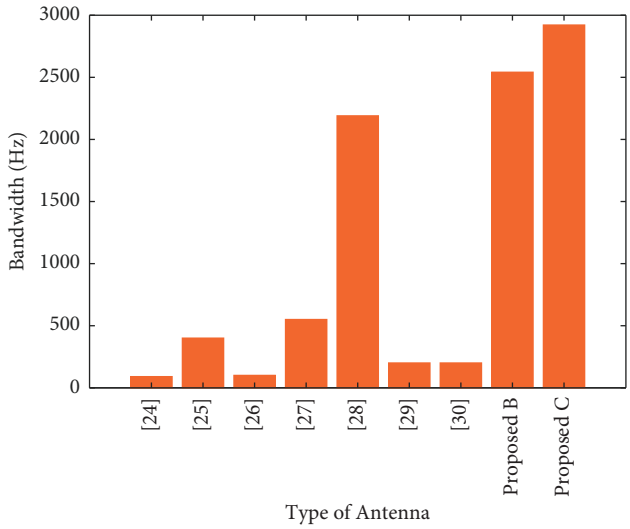

Figure 6: Bandwidth comparison chart of the proposed antenna vs. existing.

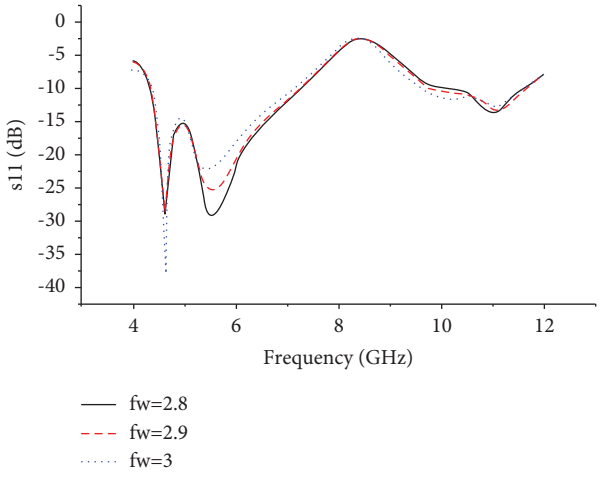

Figure 7: S11 for various fw.

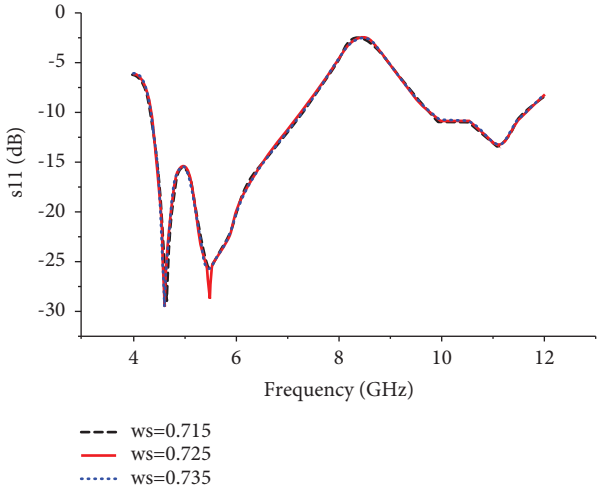

Figure 8: S11 for various ws.

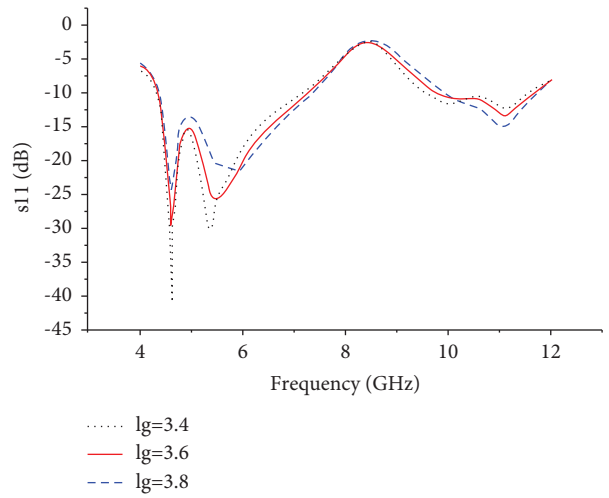

Figure 9: S11 for various lg.

phase plots of the transmission and reflection S-parameters. Figure 12 shows the permeability characteristics.

Due to its magneto-dielectric feature, as is seen in Figure 12, the SRR displays high permeability with an actual value. The enhancement in impedance bandwidth is caused by the magneto-dielectric area, which is between 4.3 GHz and 7 GHz. On the other side, this frequency band's notch is caused by the MNG area, which covers the range of 7.1 to 10.5 GHz.

5. Discussion on Proposed Antenna Results

The return loss characteristics are measured using the Agilent Vector Network Analyzer. Figure 13 shows a comparison of the observed and modelled S11 properties. A tiny difference between the simulated and measured S11 findings is seen in a higher band and may be caused by the connector's thick soldering, production tolerance, or measurement imprecision. The measured data substantially matched the simulated result.

Table 3 contains the numerical comparison for the return loss plot. Figure 14 shows the simulated co-polarization and cross-polarization of antenna C for frequencies of (a), (b), and (c), respectively, of 4.64 GHz, 5.5 GHz, and 5.5 GHz for antenna B.

The proposed antenna is analyzed in simulation and also measured in the experimental analysis. An agilent vector network analyzer is used for the analysis. The return loss feed width (F_w), slot width (W_s) in the ground, and ground height (L_g) were measured. Also, antenna B and antenna C were analyzed by considering the center frequency, refraction coefficient (S11), and bandwidth (BW). The center frequency of antenna A is 5.5 GHz, and the refraction coefficient in dB is −30.47 with a bandwidth of 2493 MHz. The antenna C has the simulated results as 5.5 GHz of center frequency, −23.73 refraction coefficient, and 2935 MHz of bandwidth.

The prototype antenna C gain is plotted in Figure 15. The proposed prototype of the antenna achieves the highest gain of 1.34 dB in the resonating band. The measured values of

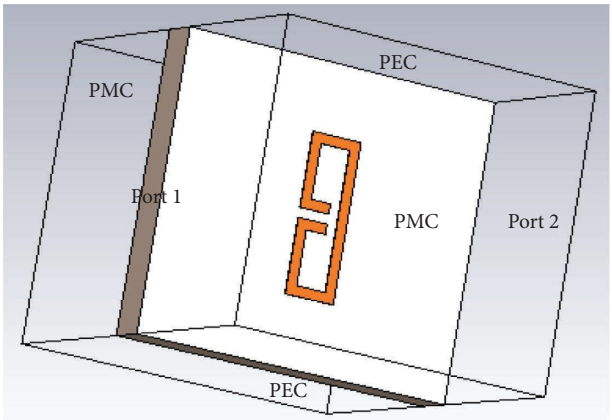

Figure 10: SRR permeability (waveguide method).

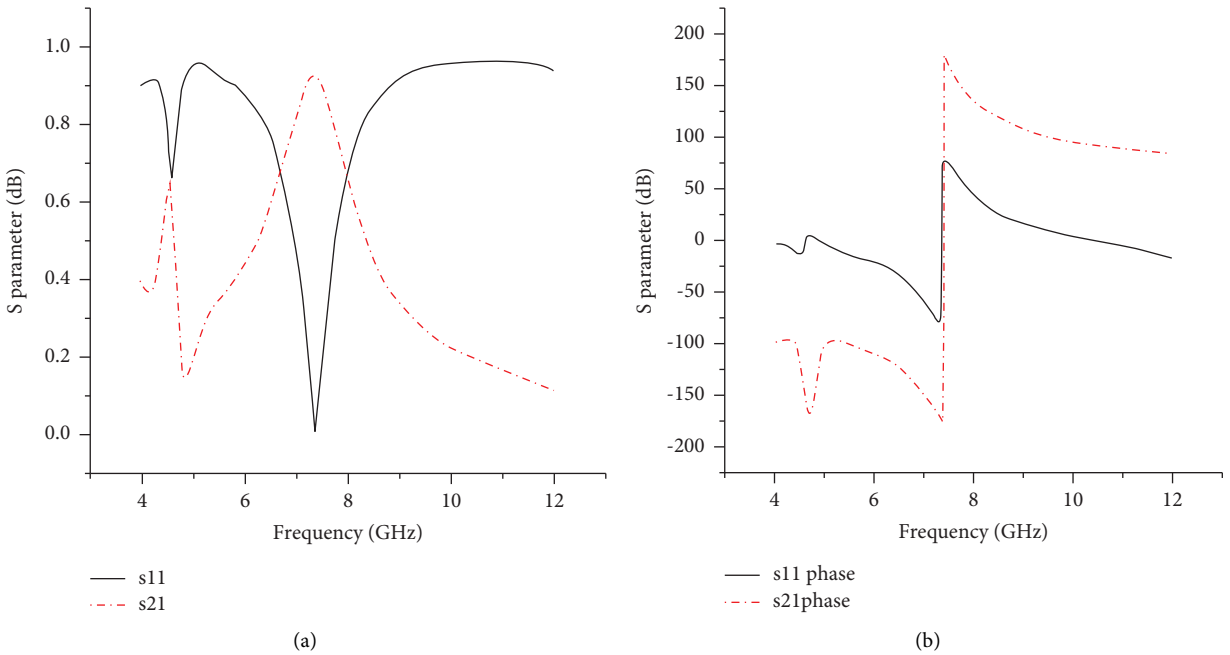

Figure 11: (a) Magnitude. (b) Phase (transmission and reflection coefficient).

the proposed antenna are 5.8 GHz of center frequency, −23.73 dB of refraction coefficient, and 2925 MHz of bandwidth. The gain by the antenna C prototype is plotted in Figure 15. This proposed antenna prototype achieves the highest gain of 1.34 dBi in the resonating band. As compared with the existing antennas discussed in the literature and comparison, the proposed antenna has the highest gain as well as less return loss. This indicates the effectiveness of the proposed antenna over the other existing antennas.

The performance of the proposed tree-shaped antenna is analyzed in terms of bandwidth, upper frequency, lower frequency, number of elements used, dimension of the antenna, permeability characteristics, return loss, refraction index, and radial pattern. The proposed structure has a resonance at 5.5 GHz (WiMAX), and the bandwidth is increased around the center frequency of 5.8 GHz after adding SRR at the substrate bottom (WLAN). The SRR is what causes the bandwidth increase, and the waveguide extraction method is used to extract the SRR's permeability

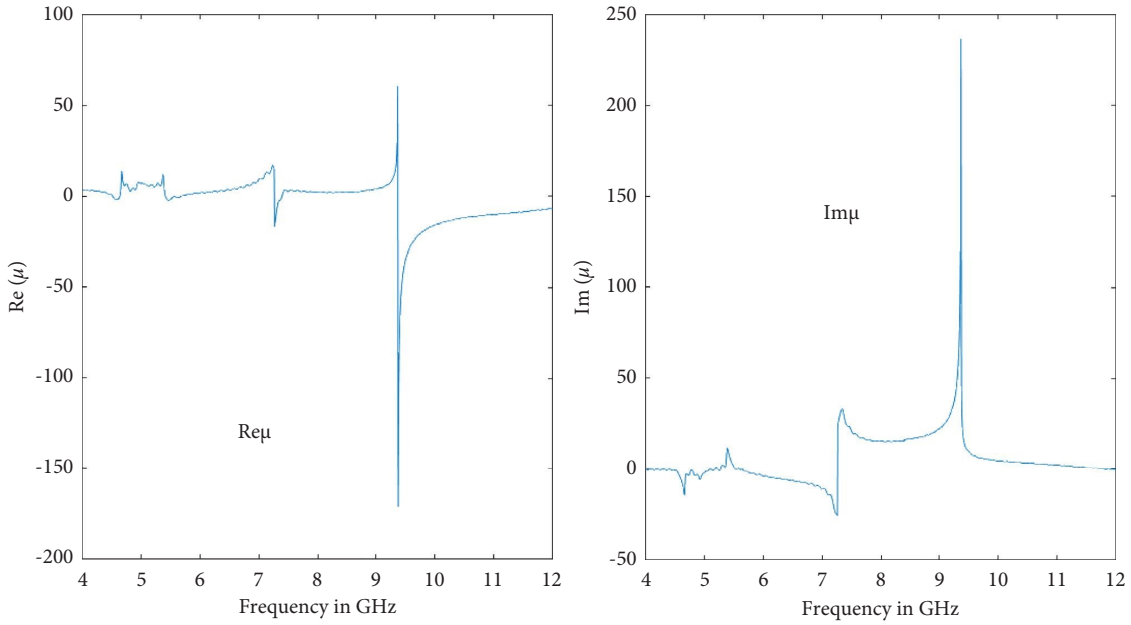

Figure 12: SRR permeability characteristics.

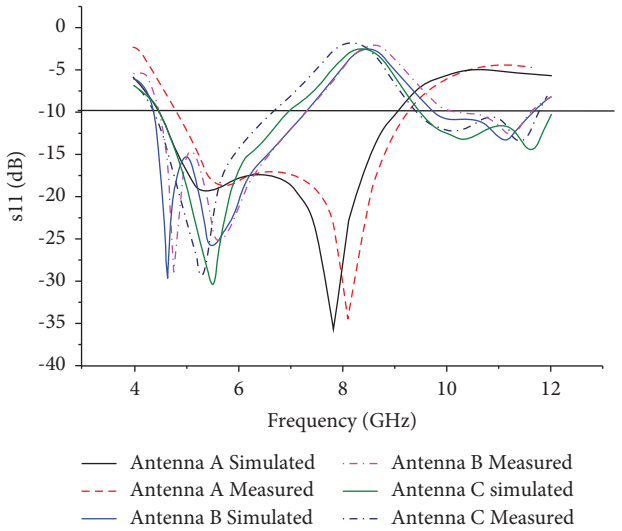

Figure 13: Measured and simulated return loss comparison plot of antenna A, B, and C.

Table 3: Assessment of the proposed antenna's simulation and measurement findings.

	Antenna proposed	SRR	Center frequency GHz	S11 dB	Bw MHz
Simulated	Antenna B	Not available	5.5	−30.47	2493
Simulated	Antenna C	Available	5.8	−23.73	2935
			10.72	−11.28	1810
Measured	Antenna C	Available	5.8	−23.73	2925
			10.72	−12.01	1801

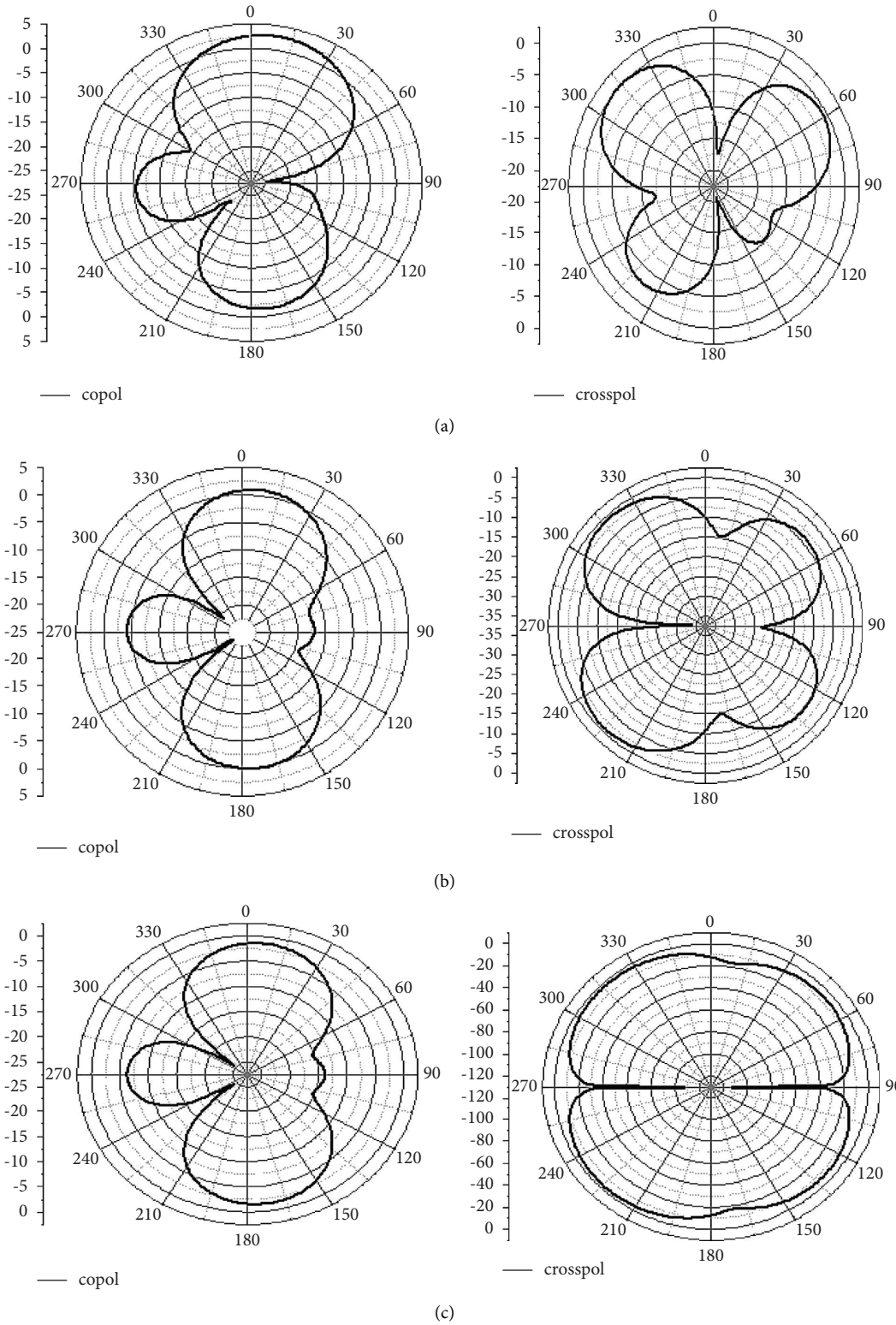

Figure 14: Radiation pattern at (a) 4.64 GHz (antenna C) (b) 5.5 GHz (antenna C) (c) 5.5 GHz (antenna B).

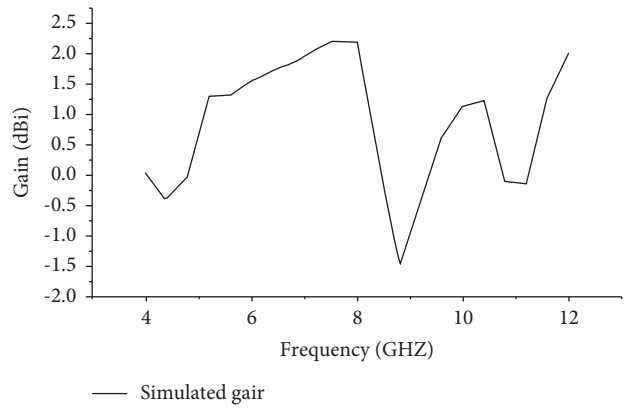

Figure 15: Simulated gain plot of antenna C.

properties. According to the parametric study, a small modification to the antenna's size might alter the properties of the proposed configuration.

6. Conclusion

A compact tree-shaped antenna is proposed for the WLAN/WiMAX application. The proposed structure operates at 5.5 GHz for WiMAX applications. Then, in order to improve the bandwidth of the proposed antenna the split-ring resonator is designed for 5.8 GHz and added at the back of the ground. The SRR is induced by the field from the patch and alters the current direction which, in turn, leads to additional frequency. The modes of the patch and SRR combined result in the bandwidth improvement of the proposed antenna. The SRR is what causes the bandwidth increase, and the waveguide extraction method is used to extract the SRR's permeability properties. The bandwidth of antenna C is 0.5 MHz greater than that of the type B antenna. Also, antenna C has an upper frequency of 4.42 GHz and a lower frequency of 7.34 GHz, whereas antenna B has an upper frequency of 4.47 GHz and a lower frequency of 7.01 GHz. According to the parametric study, a little modification to the antenna's size might alter the properties of the suggested configurations. Suggested antenna C's impedance matching is excellent, and its small size, consistent pattern, and enough gain make it a better choice for WLAN/WIMAX applications. Additionally, compared to the existing antenna, this suggested antenna has a reduced cost.

Data Availability

The data presented in this study are available upon request from the corresponding author.

Conflicts of Interest

The authors declare that there are no conflicts of interest.

References

[1] A. Kunwar, A. K. Gautam, and K. Rambabu, "Design of a compact U-shaped slot triple band antenna for WLAN/WiMAX applications," *AEU-International Journal of Electronics and Communications*, vol. 71, pp. 82–88, 2017.

[2] N. Amani, M. Kamyab, A. Jafargholi, A. Hosseinbeig, and J. S. Meiguni, "Compact tri-band metamaterial-inspired antenna based on CRLH resonant structures," *Electronics Letters*, vol. 50, no. 12, pp. 847-848, 2014.

[3] A. R. Razali and M. E. Bialkowski, "Dual-band slim inverted-F antenna with enhanced operational bandwidth," *Microwave and Optical Technology Letters*, vol. 54, no. 3, pp. 684–689, 2012.

[4] N. Rajak and N. Chattoraj, "A bandwidth enhanced metasurface antenna forwireless applications," *Microwave and Optical Technology Letters*, vol. 59, no. 10, pp. 2575–2580, 2017.

[5] J. George, C. K. Aanandan, P. Mohanan, K. G. Nair, H. Sreemoolanathan, and M. T. Sebastian, "Dielectric resonator loaded microstrip antenna for enhanced impedance bandwidth and efficiency," *Microwave and Optical Technology Letters*, vol. 17, no. 3, pp. 205–207, 1998.

[6] W. Wu, B. Yuan, B. Guan, and T. Xiang, "A bandwidth enhancement for metamaterial microstrip antenna," *Microwave and Optical Technology Letters*, vol. 59, no. 12, pp. 3076–3082, 2017.

[7] L. Peng, J. Y. Mao, X. F. Li, X. Jiang, and C. L. Ruan, "Bandwidth enhancement of microstrip antenna loaded by parasitic zeroth-order resonators," *Microwave and Optical Technology Letters*, vol. 59, no. 5, pp. 1096–1100, 2017.

[8] Y. Luo, Q. X. Chu, and J. Bornemann, "A differential-fed Yagi-Uda antenna with enhanced bandwidth via addition of parasitic resonator," *Microwave and Optical Technology Letters*, vol. 59, no. 1, pp. 156–159, 2017.

[9] S. T. Fan, Y. Z. Yin, W. Hu, B. Li, and J. H. Yang, "Bandwidth enhancement of a printed dipole antenna for wideband applications," *Microwave and Optical Technology Letters*, vol. 54, no. 7, pp. 1585–1590, 2012.

[10] S. V. Reddy, D. Sarkar, K. Saurav, and K. V. Srivastava, "LC resonator loaded bandwidth enhanced tri-band planar inverted-F antenna," *Microwave and Optical Technology Letters*, vol. 57, no. 8, pp. 1879–1883, 2015.

[11] V. Rajeshkumar and S. Raghavan, "Bandwidth enhanced compact fractal antenna for UWB applications with 5-6 GHz band rejection," *Microwave and Optical Technology Letters*, vol. 57, no. 3, pp. 607–613, 2015.

[12] A. Mehdipour, T. A. Denidni, and A. R. Sebak, "Multiband miniaturized antenna loaded by ZOR and CSRR metamaterial structures with monopolar radiation pattern," *IEEE Transactions on Antennas and Propagation*, vol. 62, no. 2, pp. 555–562, 2014.

[13] M. Yoo and S. Lim, "SRR and CSRR loaded ultra-wideband (UWB) antenna with tri-band notch capability," *Journal of Electromagnetic Waves and Applications*, vol. 27, no. 17, pp. 2190–2197, 2013.

[14] H. X. Xu, G. M. Wang, C. X. Zhang, and Q. Peng, "Hilbert shaped complementary single split ring resonator and low-pass filter with ultra-wide stopband, excellent selectivity and low insertion loss," *AEU - International Journal of Electronics and Communications*, vol. 65, no. 11, pp. 901–905, 2011.

[15] H. Memarzadeh-Tehran, R. Abhari, and M. Niayesh, "A cavity backed antenna loaded with complimentary split ring resonators," *AEU - International Journal of Electronics and Communications*, vol. 70, no. 7, pp. 928–935, 2016.

[16] K. V. Phani Kumar and S. S. Karthikeyan, "Wideband three section branch line coupler using triple open complementary split ring resonator and open stubs," *AEU - International*

Journal of Electronics and Communications, vol. 69, no. 10, pp. 1412–1416, 2015.

[17] C. Caloz and T. Itoh, *Electromagnetic Metamaterials Transmission Line Theory and Microwave Applications*, John Wiley Sons, Inc, New York, NY,USA, 2006.

[18] P. J. C. Sam and N. Gunavathi, "A tri-band monopole antenna loaded with circular electric–inductive–capacitive metamaterial resonator for wireless application," *Applied Physics A*, vol. 126, p. 774, 2020.

[19] M. J. Asad, M. F. Shafique, and S. A. Khan, "Performance restoration of dielectric embedded antennas using omega like complementary split ring resonators," *Microwave and Optical Technology Letters*, vol. 59, no. 2, pp. 357–362, 2017.

[20] S. Prasad Jones Christydass and N. Gunavathi, "Dual-band complementary split-ring resonator engraved rectangular monopole for GSM and WLAN/WiMAX/5G sub-6 GHz band (new radio band)," *Progress in Electromagnetics Research C*, vol. 113, pp. 251–263, 2021.

[21] R. Boopathi Rani and S. K. Pandey, "Metamaterial inspired printed UWB antenna for short range RADAR applications," *Microwave and Optical Technology Letters*, vol. 59, no. 7, pp. 1600–1604, 2017.

[22] S. Choudhury and A. Mohan, "Miniaturized Sierpinski fractal loaded QMSIW antenna with CSRR in ground plane for WLAN applications," *Microwave and Optical Technology Letters*, vol. 59, no. 6, pp. 1291–1295, 2017.

[23] S. Prasad Jones Christydass and N. Gunavathi, "Octa-band metamaterial inspired multiband monopole antenna for wireless application," *Progress in Electromagnetics Research C*, vol. 113, pp. 97–110, 2021.

[24] M. A. Abdalla and A. A. Ibrahim, "Compact and closely spaced Metamaterial MIMO antenna with high isolation for wireless applications," *IEEE Antennas and Wireless Propagation Letters*, vol. 12, pp. 1452–1455, 2013.

[25] S. M. Alqadami, M. F. Jamlos, P. J. Soh, and G. A. E. Vandenbosch, "Assessment of PDMS technology in a MIMO antenna array," *IEEE Antennas and Wireless Propagation Letters*, vol. 15, pp. 1939–1942, 2016.

[26] X. Sun and M. Y. Cao, "Low mutual coupling antenna array for WLAN application," *Electronics Letters*, vol. 53, no. 6, pp. 368–370, 2017.

[27] C. Mahatthanajatuphat, S. Saleekaw, P. Akkaraekthalin, and M. Krairiksh, "A rhombic patch monopole antenna with modified minkowski fractal geometry for UMTS, WLAN, and mobile WiMAX application," *Progress in Electromagnetics Research*, vol. 89, pp. 57–74, 2009.

[28] R. Zaker, C. Ghobadi, and J. Nourinia, "A modified microstrip-fed two-step tapered monopole antenna for UWB and WLAN applications," *Progress in Electromagnetics Research*, vol. 77, pp. 137–148, 2007.

[29] Y.-J. Wu, B.-H. Sun, J.-F. Li, and Q.-Z. Liu, "Triple-band omni-directional antenna for WLAN application," *Progress in Electromagnetics Research*, vol. 76, pp. 477–484, 2007.

[30] S. Lakrit, A. Nella, S. Das, B. T. P. Madhav, and C. Murali Krishna, "An integrated three-antenna structure for 5G, WLAN, LTE and ITU band cognitive radio communication," *AEU - International Journal of Electronics and Communications*, vol. 139, Article ID 153906, 2021.

[31] D. P. Mishra and S. K. Behera, "Modified rectangular resonators based multi-frequency narrow-band RFID reader antenna," *Microwave and Optical Technology Letters*, vol. 64, pp. 544–551, 2022.

[32] R. Azim, K. Dhar, M. S. Mia, and M. T. Islam, "Inset-fed microstrip patch antenna for ubiquitous wireless communication applications," *International Journal of Ultra Wideband Communications and Systems*, vol. 5, pp. 57–64, 2022.

[33] A. Ghaffar, W. A. Awan, N. Hussain, S. Ahmad, and X. J. Li, "A compact dual-band flexible antenna for applications at 900 and 2450 MHZ," *Progress In Electromagnetics Research Letters*, vol. 99, pp. 83–91, 2021.